





Quench dynamics and relaxation of a spin coupled to interacting leads

Helena Bragança ^{1,2}, M. F. Cavalcante ², R. G. Pereira ³ and Maria C. O. Aguiar ²

¹*Instituto de Física and International Center for Physics, Universidade de Brasília, Brasília 70919-970, DF, Brazil*

²*Departamento de Física, Universidade Federal de Minas Gerais, C. P. 702, 30123-970 Belo Horizonte, MG, Brazil*

³*International Institute of Physics and Departamento de Física Teórica e Experimental, Universidade Federal do Rio Grande do Norte, 59072-970 Natal-RN, Brazil*



(Received 22 January 2021; accepted 11 March 2021; published 25 March 2021)

We study a quantum quench in which a magnetic impurity is suddenly coupled to Hubbard chains, whose low-energy physics is described by Tomonaga-Luttinger liquid theory. Using the time-dependent density-matrix renormalization-group (tDMRG) technique, we analyze the propagation of charge, spin, and entanglement in the chains after the quench and relate the light-cone velocities to the dispersion of holons and spinons. We find that the local magnetization at the impurity site decays faster if we increase the interaction in the chains, even though the spin velocity decreases. We derive an analytical expression for the relaxation of the impurity magnetization which is in good agreement with the tDMRG results at intermediate timescales, providing valuable insight into the time evolution of the Kondo screening cloud in interacting systems.

DOI: [10.1103/PhysRevB.103.125152](https://doi.org/10.1103/PhysRevB.103.125152)

I. INTRODUCTION

The interaction between a magnetic impurity and a non-magnetic metallic host is one of the fundamental problems in many-body physics [1]. A deep understanding of the Kondo effect has been achieved thanks to the numerical renormalization group [2], the exact Bethe ansatz solution [3], and conformal field theory techniques [4]. A hallmark of the Kondo effect is the emergence of a characteristic scale, the Kondo temperature T_K , which varies exponentially with the exchange coupling between the impurity and a Fermi liquid metal. At temperatures below T_K , perturbation theory in the exchange coupling breaks down, and the properties of the system are governed by the formation of a singlet state between the impurity and the conduction electrons [5]. Kondo physics is also manifested in the spatial dependence of spin correlations [6–11], which change qualitatively over distances of the order of $\xi_K = \hbar v_F / (k_B T_K)$, where v_F is the Fermi velocity of the conduction electrons and \hbar and k_B are the Planck and Boltzmann constants, respectively. The length scale ξ_K is interpreted as the size of the Kondo screening cloud, whose effects have been observed recently in a mesoscopic device [12].

Experiments with quantum dots coupled to electron reservoirs [13,14] opened the way for controllable realizations and inspired studies of the nonequilibrium dynamics of Kondo systems [15–23]. The active research on this topic has also been boosted by recent efforts to simulate the Kondo effect with ultracold atoms [24–27]. A typical quench protocol in this context consists of switching on the coupling between an initially spin-polarized impurity and a metallic lead [15,28–30]. One then observes a real-time decay of the impurity magnetization accompanied by the buildup of Kondo correlations over a time scale $\tau_K = \hbar / (k_B T_K)$ after the quench. By analogy with the Kondo effect, the scaling behavior in the

time dependence as the system approaches equilibrium has also been studied for the resonant level model [31–33].

The usual description of the Kondo effect within the single-impurity Anderson model [1] takes into account the local interaction at the quantum dot but neglects electron-electron interactions in the bulk. In higher dimensions, this approximation is justified by Landau's Fermi liquid theory, where the bulk degrees of freedom are associated with weakly interacting fermionic quasiparticles. However, if the leads are interacting one-dimensional systems, as in the case of quantum wires [34], Fermi liquid theory must be replaced by Tomonaga-Luttinger liquid (TLL) theory [35]. In a TLL, the elementary excitations are spin-charge-separated bosonic modes and correlation functions decay as power laws with interaction-dependent exponents. Despite the spin-charge separation in the bulk, the Kondo effect in a TLL can still be affected by interactions in the charge sector [36–41].

In this work we investigate the nonequilibrium dynamics after a local quench in which a spin-polarized electron is suddenly coupled to a correlated chain described by a repulsive Hubbard model. We are particularly interested in comparing numerical results obtained by time-dependent density matrix renormalization group (tDMRG) methods with the predictions from an effective field theory for the coupling of a localized spin to a TLL. We first study the problem using bosonization to describe the quench within TLL theory, following the approach of Ref. [42]. Applying perturbation theory in the Kondo coupling J_K , we derive an analytical expression for the decay of the impurity magnetization valid up to intermediate times, which are greater than the microscopic time scale \hbar/J_K but shorter than the Kondo time τ_K . Second, we simulate the nonequilibrium dynamics in the lattice model using tDMRG. Analyzing the propagation of correlations and entanglement entropy, we observe two light cones with distinct velocities, which can be identified with the maximum velocities of

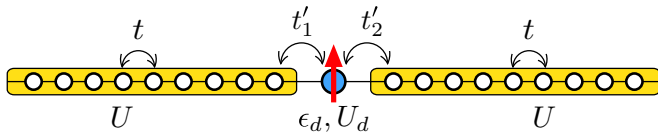


FIG. 1. Schematic representation of the quantum quench in the Anderson impurity model with interacting leads. At the initial time, the impurity site with energy ϵ_d and interaction U_d , occupied by a spin-up electron, is connected to the left and right wires via hybridization couplings t'_1 and t'_2 , respectively. The wires are described by a quarter-filled Hubbard model with hopping parameter t and onsite interaction U .

elementary charge and spin excitations in the Hubbard chain. The numerical results confirm the field theory prediction of a time regime where the impurity magnetization scales logarithmically with time. On the other hand, they also reveal a strong dependence on the interaction strength which we ascribe to a renormalization of the high-energy cutoff in the field theory, rather than to the Luttinger parameter in the charge sector.

The remainder of the paper is organized as follows. In Sec. II, we introduce the time-dependent Anderson impurity model with interacting leads and describe the quench protocol. In Sec. III, we use the TLL theory to derive an analytical expression for the real-time decay of the impurity magnetization from perturbation theory in the Kondo coupling. Section IV presents our tDMRG results. We discuss the propagation of perturbations after the quench in relation to the exact velocities of elementary excitations and analyze the relaxation of local observables at the impurity site. Our concluding remarks can be found in Sec. V. Finally, Appendix contains some details of the analytical calculation outlined in Sec. III. Hereafter we set $\hbar = k_B = 1$.

II. MODEL AND QUENCH PROTOCOL

We consider the setup shown in Fig. 1, described by the time-dependent Hamiltonian

$$H(\tau) = H_{\text{leads}} + H_{\text{imp}} + \Theta(\tau)H_{\text{hyb}}, \quad (1)$$

where $\Theta(\tau)$ denotes the Heaviside step function. The first term represents the Hamiltonian for the conduction electrons in the interacting leads, $H_{\text{leads}} = \sum_{\ell=1}^2 H_{\ell}$, where the index $\ell = 1, 2$ labels the left and right wires, respectively. Each wire is described by a Hubbard model:

$$H_1 = -t \sum_{i=-L_1}^{-2} \sum_{\sigma} (c_{i\sigma}^{\dagger} c_{i+1\sigma} + \text{H.c.}) + U \sum_{i=-L_1}^{-1} n_{i\uparrow} n_{i\downarrow},$$

$$H_2 = -t \sum_{i=1}^{L_2-1} \sum_{\sigma} (c_{i\sigma}^{\dagger} c_{i+1\sigma} + \text{H.c.}) + U \sum_{i=1}^{L_2} n_{i\uparrow} n_{i\downarrow}, \quad (2)$$

where $c_{i\sigma}$ annihilates an electron with spin $\sigma = \uparrow, \downarrow$ at site i , $n_{i\sigma} = c_{i\sigma}^{\dagger} c_{i\sigma}$ are number operators, t is the hopping parameter, and $U > 0$ is the onsite interaction strength. The number of sites is L_1 for the chain on the left and L_2 for the chain on the right, and we impose open boundary conditions at the chain ends. Throughout this work, we set $t = 1$, which defines the unit of energy. We shall work at fixed average density

$\rho = N_1/L_1 = N_2/L_2$, where N_{ℓ} is the number of electrons in each decoupled chain in the initial state. At half filling, an infinitesimal $U > 0$ drives the system into a Mott insulating phase [35]. To consider interacting metallic leads, we set the density to quarter filling, $\rho = 1/2$.

The Hamiltonian for the impurity site, $i = 0$, is given by

$$H_{\text{imp}} = \epsilon_d n_0 + U_d n_{0\uparrow} n_{0\downarrow}, \quad (3)$$

where $n_0 = n_{0\uparrow} + n_{0\downarrow}$, ϵ_d is the energy shift of the localized state with respect to the Fermi level in the leads, and U_d is the local interaction. To have a local moment at the impurity site, we consider $\epsilon_d < 0$ and $U_d > 0$.

Finally, the hybridization between the impurity and the chains is described by

$$H_{\text{hyb}} = -t'_1 \sum_{\sigma} c_{-1\sigma}^{\dagger} c_{0\sigma} - t'_2 \sum_{\sigma} c_{0\sigma}^{\dagger} c_{1\sigma} + \text{H.c.}, \quad (4)$$

where t'_1 and t'_2 are the hopping parameters between the impurity site and the nearest sites in the left or right chains, respectively. While this model describes the general case of asymmetric tunneling amplitudes, we shall focus on two special limits. First, in the maximally asymmetric case, we set $t'_1 = 0$ and $t'_2 \neq 0$. The impurity site is then coupled only to the first site of the right wire and we can forget about the left wire. Second, for $t'_1 = t'_2$, the impurity site is coupled symmetrically to both wires. In this case, hopping through the impurity site allows for electron transport between the wires.

We are mainly interested in the strong Coulomb blockade regime $t'_{1,2} \ll -\epsilon_d, U_d$, where states in the low-energy subspace contain a singly occupied impurity site, $n_0 = 1$. We then apply a Schrieffer-Wolff transformation to integrate out high-energy processes that change the occupation of the impurity site [1]. As a result, model (1) can be mapped onto the effective Hamiltonian

$$H_{\text{eff}}(\tau) = H_{\text{leads}} + \Theta(\tau)H_K, \quad (5)$$

where [43]

$$H_K = J_K \mathbf{S}_0 \cdot (\kappa_1 c_{-1}^{\dagger} + \kappa_2 c_1^{\dagger}) \frac{\boldsymbol{\sigma}}{2} (\kappa_1 c_{-1} + \kappa_2 c_1) + V (\kappa_1 c_{-1}^{\dagger} + \kappa_2 c_1^{\dagger}) (\kappa_1 c_{-1} + \kappa_2 c_1). \quad (6)$$

Here $\mathbf{S}_0 = c_0^{\dagger} (\boldsymbol{\sigma}/2) c_0$ is the spin operator for the electron at the impurity site and $\boldsymbol{\sigma}$ is the vector of Pauli matrices acting on the two-component spinor $c_i = (c_{i\uparrow}, c_{i\downarrow})^t$. The antiferromagnetic Kondo coupling $J_K > 0$ is given by

$$J_K = 2[(t'_1)^2 + (t'_2)^2] \left(\frac{1}{-\epsilon_d} + \frac{1}{U_d + \epsilon_d} \right), \quad (7)$$

and the amplitude V of the potential scattering term is given by

$$V = \frac{(t'_1)^2 + (t'_2)^2}{2} \left(\frac{1}{-\epsilon_d} - \frac{1}{U_d + \epsilon_d} \right). \quad (8)$$

The dimensionless parameters $\kappa_{1,2}$ in Eq. (6) are

$$\kappa_1 = \frac{t'_1}{\sqrt{(t'_1)^2 + (t'_2)^2}}, \quad \kappa_2 = \frac{t'_2}{\sqrt{(t'_1)^2 + (t'_2)^2}}. \quad (9)$$

For $t'_1 = 0$ and $t'_2 \neq 0$, the impurity spin couples to the spin density at the boundary of the right wire. For $t'_1 = t'_2$, it

couples to the symmetric orbital at sites $i = \pm 1$. The potential scattering can be canceled at lowest order in $t'_{1,2}/U_d$ if we set $\epsilon_d = -U_d/2$. Note, however, that a nonzero V may be generated at higher orders because particle-hole symmetry is broken for any electron density away from half filling.

In the quench protocol, we assume that for times $\tau < 0$ the system is prepared in the state

$$|\Psi_0\rangle = |\text{GS}\rangle_1 \otimes |\uparrow\rangle \otimes |\text{GS}\rangle_2, \quad (10)$$

where $|\text{GS}\rangle_\ell$ for $\ell = 1, 2$ is the ground state of the disconnected Hubbard chains and $|\uparrow\rangle$ is the polarized state of the impurity spin. This initial state is not an eigenstate of Hamiltonian (1) for $\tau > 0$. After we switch on the hybridization couplings, the state evolves nontrivially according to

$$|\Psi(\tau)\rangle = e^{-i\tau(H_{\text{leads}}+H_{\text{imp}}+H_{\text{hyb}})}|\Psi_0\rangle. \quad (11)$$

Since this is a local quench, we expect that, in the thermodynamic limit and for sufficiently long times, local observables will relax to the corresponding expectation values in the ground state of the post-quench Hamiltonian. The ground state of $H(\tau > 0)$ in Eq. (1) at quarter filling was studied numerically in Ref. [44]. For noninteracting chains, $U = 0$, one finds that the Kondo regime, where $\langle n_0 \rangle \approx 1$ and $\langle (S_0^z)^2 \rangle \approx 1/4$, is reached with good approximation for $t' = 0.5$ and $U_d \gtrsim 5$. Smaller values of U_d lead to a mixed valence regime with significant deviations from single occupancy in the impurity site. Importantly, for a fixed value of U_d , increasing the interaction $U > 0$ in the chains suppresses charge fluctuations and drives the system closer to the Kondo regime [44].

III. FIELD THEORY APPROACH

Deep in the Kondo regime, we can use the Hamiltonian in Eq. (5) to study the time evolution of observables which do not entail charge fluctuations at the impurity site. In particular, we shall be interested in the time-dependent impurity magnetization

$$m_0(\tau) = \langle \Psi(\tau) | S_0^z | \Psi(\tau) \rangle. \quad (12)$$

The latter must decay to zero for $\tau \rightarrow \infty$, signaling the formation of the Kondo screening cloud. In this section, we calculate the time dependence of $m_0(\tau)$ using the low-energy effective field theory and perturbation theory in the Kondo coupling. Our calculation for electrons with spin is inspired by the approach of Ref. [42] for spinless fermions.

A. Effective Hamiltonian

We start with the Luttinger model for the disconnected interacting leads. Here we consider two semi-infinite chains, corresponding to the limit $L_{1,2} \rightarrow \infty$. To describe the low-energy modes in the wires, we take the continuum limit and expand the fermionic field operators in terms of right (R) and left (L) movers [35]

$$c_{j\sigma} \sim c_{\ell,\sigma}(x) = e^{ik_F x} \psi_{R,\ell,\sigma}(x) + e^{-ik_F x} \psi_{L,\ell,\sigma}(x), \quad (13)$$

where $c_{1,\sigma}(x)$ is defined for $x < 0$ and $c_{2,\sigma}(x)$ for $x > 0$. At quarter filling, the Fermi momentum is $k_F = \pi/4$, where we set the lattice spacing to unity. The open boundary condition, $c_{\ell,\sigma}(0) = 0$, can be cast as a constraint on the chiral fermionic

modes in each wire [39]

$$\psi_{L,\ell,\sigma}(x) = -\psi_{R,\ell,\sigma}(-x). \quad (14)$$

Thus, for instance, the left mover in wire $\ell = 2$ can be regarded as the analytic continuation of the right mover to the negative- x axis. Likewise, we may choose the right mover in wire $\ell = 1$ to be the analytic continuation of the corresponding left mover to the positive- x axis. These relations allow us to work with a single chiral field in each wire redefined in the domain $x \in \mathbb{R}$. It will be convenient to use the two-component spinors

$$\begin{aligned} \psi_1^\dagger(x) &= (\psi_{L,1,\uparrow}^\dagger(-x), \psi_{L,1,\downarrow}^\dagger(-x)), \\ \psi_2^\dagger(x) &= (\psi_{R,2,\uparrow}^\dagger(x), \psi_{R,2,\downarrow}^\dagger(x)). \end{aligned} \quad (15)$$

In the continuum limit, the Hamiltonian for the interacting leads becomes the Luttinger model with an open boundary [39], $H_\ell \approx H_\ell^{\text{LL}}$, with

$$\begin{aligned} H_\ell^{\text{LL}} &= v_F \int_{-\infty}^{\infty} dx \left[\psi_\ell^\dagger(-i\partial_x) \psi_\ell \right. \\ &\quad \left. + \frac{g}{2} \rho_\ell(x) \rho_\ell(x) + \frac{g}{2} \rho_\ell(x) \rho_\ell(-x) \right], \end{aligned} \quad (16)$$

where $v_F = 2 \sin k_F$ is the Fermi velocity of the noninteracting system, $g = U/v_F$ is a dimensionless parameter, and $\rho_\ell = \psi_\ell^\dagger \psi_\ell$ is a density operator.

Using Abelian bosonization [35,45], we write the fermionic field in terms of charge and spin boson fields:

$$\psi_\ell(x) \sim \frac{1}{\sqrt{2\pi\alpha}} \begin{pmatrix} e^{-i\sqrt{\frac{\alpha}{2}}[\phi_{\ell,c}(x)+\phi_{\ell,s}(x)]} \\ e^{-i\sqrt{\frac{\alpha}{2}}[\phi_{\ell,c}(x)-\phi_{\ell,s}(x)]} \end{pmatrix}, \quad (17)$$

where α is a short-distance cutoff and $\phi_{\ell,c/s} = (\phi_{\ell,\uparrow} \pm \phi_{\ell,\downarrow})/\sqrt{2}$ obey the commutation relations

$$[\phi_{\ell,\lambda}(x), \phi_{\ell',\lambda'}(y)] = i\delta_{\ell\ell'} \delta_{\lambda\lambda'} \text{sgn}(x-y). \quad (18)$$

In terms of bosonic annihilation operators $\eta_{\ell,\lambda,q}$ with momentum $q > 0$, the fields $\phi_{\ell,\lambda}(x)$ are given by

$$\phi_{\ell,\lambda}(x) = \frac{1}{\sqrt{L}} \sum_{q>0} \frac{e^{-\frac{q}{2}x}}{\sqrt{q}} [z_{\lambda,q}(x) \eta_{\ell,\lambda,q} + z_{\lambda,q}^*(x) \eta_{\ell,\lambda,q}^\dagger], \quad (19)$$

where $z_{\lambda,q}(x) = (1/\sqrt{K_\lambda}) \cos(qx) + i\sqrt{K_\lambda} \sin(qx)$, with K_λ the Luttinger parameter in the charge or spin sector for $\lambda = c, s$, respectively. The SU(2) spin-rotation symmetry of the Hamiltonian for the leads fixes $K_s = 1$ [35,45]. For the charge sector, bosonization gives $K_c \approx 1 - g/\pi$ to first order in $g \ll 1$. The exact value of the charge Luttinger parameter can be obtained from the Bethe ansatz solution of the Hubbard model [46,47]. For repulsive interactions, one finds $K_c < 1$, with $K_c = 1$ for $U = 0$ and $K_c \rightarrow 1/2$ for $U \rightarrow \infty$. Using the mode expansion in Eq. (19), we diagonalize the Luttinger Hamiltonian in the form

$$H_\ell^{\text{LL}} = \sum_{\lambda=c,s} \sum_{q>0} v_{\lambda,q} \eta_{\ell,\lambda,q}^\dagger \eta_{\ell,\lambda,q}, \quad (20)$$

with $v_{c/s}$ being the velocities of the charge and spin bosonic modes. Like the Luttinger parameters, the exact velocities can be determined using the Bethe ansatz solution. In particular, in the strong coupling limit $U \rightarrow \infty$, the ground-state wave

function can be expressed as a product of a Slater determinant of spinless fermions and the spin wave function of the spin-1/2 Heisenberg chain [48]. In this limit, the spin velocity vanishes, $v_s \sim t^2/U \rightarrow 0$, while the charge velocity approaches $v_c = 2 \sin k_F$ [48,49].

The Kondo coupling involves the fermionic fields at sites $i = \pm 1$. Using the boundary condition, we get

$$\begin{aligned} c_{1\sigma} &\sim e^{ik_F} \psi_{R,2,\sigma}(0) + e^{-ik_F} \psi_{L,2,\sigma}(0) \\ &= 2i \sin k_F \psi_{R,2,\sigma}(0). \end{aligned} \quad (21)$$

Likewise, $c_{-1\sigma} \sim 2i \sin k_F \psi_{L,1,\sigma}(0)$. We can now write the Kondo coupling in the weak coupling limit $J_K \ll t$. We will distinguish between the two cases of interest. First, for $t'_1 = 0$ we obtain

$$H_K^{(1)} = \lambda_K \mathbf{S}_0 \cdot \psi_2^\dagger(0) \frac{\boldsymbol{\sigma}}{2} \psi_2(0) :, \quad (22)$$

where $: \dots :$ denotes normal ordering and we have used $k_F = \pi/4$ and $\epsilon_d = -U_d/2$ to obtain the bare Kondo coupling $\lambda_K = 4J_K \sin^2 k_F = 16(t'_2)^2/U_d$ to lowest order in t'_2/U_d . Second, for $t'_1 = t'_2$, we obtain

$$H_K^{(2)} = \lambda_K \mathbf{S}_0 \cdot \sum_{\ell, \ell'} \psi_\ell^\dagger(0) \frac{\boldsymbol{\sigma}}{2} \psi_{\ell'}(0) :, \quad (23)$$

with the same bare λ_K as in Eq. (22). Note that the terms with $\ell \neq \ell'$ in $H_K^{(2)}$ account for processes which transfer electrons between the wires.

In bosonized form, the Kondo Hamiltonian for the impurity coupled to a single wire becomes

$$\begin{aligned} H_K^{(1)} &= \frac{\lambda_K}{2} \left[S_0^+ \frac{e^{-i\sqrt{2\pi}\phi_{2s}(0)}}{2\pi\alpha} + S_0^- \frac{e^{i\sqrt{2\pi}\phi_{2s}(0)}}{2\pi\alpha} \right. \\ &\quad \left. + S_0^z \frac{1}{\sqrt{2\pi}} \partial_x \phi_{2s}(0) \right]. \end{aligned} \quad (24)$$

In this case, the Kondo interaction does not involve the charge boson. In fact, spin-charge separation is preserved when the impurity spin is coupled to the open boundary of a TLL [39,50]. As a consequence, the equilibrium Kondo effect in this geometry does not exhibit anomalous scaling associated with the Luttinger parameter $K_c < 1$ in the charge sector. This is in contrast to the Kondo effect in a TLL studied in Refs. [36,37], where the impurity spin is coupled to the electron spin density in the middle of an infinite wire. However, the Kondo effect described by Eq. (24) can still be affected by interactions in the bulk as the latter can renormalize the bare Kondo coupling λ_K or equivalently the nonuniversal constant α in prefactor of the boundary spin operators. We shall see that is indeed the case when we analyze the numerical results in Sec. IV.

When the impurity spin is symmetrically coupled to both wires, we obtain

$$H_K^{(2)} = \frac{\lambda_K}{2} (S_0^+ F + S_0^- F^\dagger + S_0^z G), \quad (25)$$

where the boundary operators F and G are given by

$$\begin{aligned} F &= \frac{1}{2\pi\alpha} [e^{-i\sqrt{2\pi}\phi_{1s}(0)} + e^{-i\sqrt{2\pi}\phi_{2s}(0)}] \\ &\quad + C \frac{e^{-i\sqrt{\pi}\phi_s^+(0)}}{\pi\alpha} \cos[\sqrt{\pi}\phi_c^-(0)], \quad (26) \\ G &= \sqrt{\frac{1}{\pi}} \partial_x \phi_s^+(0) - \frac{2C}{\pi\alpha} \sin[\sqrt{\pi}\phi_c^-(0)] \sin[\sqrt{\pi}\phi_s^-(0)]. \end{aligned} \quad (27)$$

Here $\phi_\lambda^\pm = (\phi_{1\lambda} \pm \phi_{2\lambda})/\sqrt{2}$ are symmetric and antisymmetric combinations with respect to exchanging the wires. In addition to the spin-only terms analogous to Eq. (24), the Kondo interaction for this geometry contains operators that involve the charge bosons and are associated with tunneling between the wires. Here we have introduced a nonuniversal constant C because the tunneling terms renormalize differently than the ones that scatter electrons back into the same wire [39]. Given that the Kondo interaction involves the charge boson, in this case we should expect some explicit interaction dependence as the Luttinger parameter K_c must show up in the exponent of correlators for the boundary operators.

B. Decay of the impurity magnetization after the quantum quench

We now turn to the calculation of $m_0(\tau)$. In the effective field theory, the ground state of the disconnected leads is a vacuum of the bosonic modes of the TLLs. Thus, the initial state is written as $|\Psi_0\rangle = |0\rangle_1 \otimes |\uparrow\rangle \otimes |0\rangle_2$, where $|0\rangle_\ell$ for $\ell = 1, 2$ obey $\eta_{\ell,\lambda,q}|0\rangle_\ell = 0$ for both spin and charge modes ($\lambda = c, s$) and any $q > 0$.

Let us first consider the case in which the impurity is coupled to a single wire. The time evolution for $\tau > 0$ is governed by the effective Hamiltonian $H_0 + H_K^{(1)}$, with $H_0 = H_2^{\text{LL}}$. In the interaction picture, we write

$$m_0(\tau) = \langle \Psi_I(\tau) | S_{0,I}^z(\tau) | \Psi_I(\tau) \rangle. \quad (28)$$

Here $\hat{O}_I(\tau) = e^{iH_0\tau} \hat{O} e^{-iH_0\tau}$ denotes an operator evolved with the unperturbed Hamiltonian, while the state evolves with the Kondo interaction in the form

$$|\Psi_I(\tau)\rangle = T \exp \left[-i \int_0^\tau d\tau' H_{K,I}^{(1)}(\tau') \right] |\Psi_0\rangle, \quad (29)$$

where T denotes time ordering.

Clearly, the initial condition is $m_0(0) = 1/2$. Expanding the exponential in Eq. (29) in powers of the Kondo coupling λ_K , we find that the first nonvanishing correction appears at order J_K^2 . Following the steps detailed in Appendix, we obtain

$$m_0(\tau) \approx \frac{1}{2} - \frac{\lambda_K^2}{4} \int_0^\tau d\tau' d\tau'' C(\tau' - \tau'') + \mathcal{O}(\lambda_K^3), \quad (30)$$

where $C(\tau) = (2\pi\alpha)^{-2} \langle e^{-i\sqrt{2\pi}\phi_{2s}(0,\tau)} e^{i\sqrt{2\pi}\phi_{2s}(0,0)} \rangle_0$ and $\langle \dots \rangle_0$ denotes the expectation value in $|\Psi_0\rangle$. Calculating the correlator and performing the integration over τ' and τ'' , we obtain a logarithmic dependence for the time decay:

$$m_0(\tau) = \frac{1}{2} - \left(\frac{\lambda_K}{4\pi\alpha\Lambda} \right)^2 \ln[1 + (\Lambda\tau)^2] + \mathcal{O}(\lambda_K^3), \quad (31)$$

where $\Lambda \sim v_F/\alpha$ is an ultraviolet cutoff that appears in the boundary correlators. Note that the leading time dependence of $m_0(\tau)$ stems from the correlator for the operators associated with spin-flip scattering in Eq. (24), which provides a mechanism for the relaxation of the polarized impurity spin.

According to the perturbative result in Eq. (31), the impurity magnetization would vanish for times $\tau \sim \Lambda^{-1} e^{8\pi^2(\alpha\Lambda/\lambda_K)^2} \gg \Lambda^{-1}$. However, we expect the lowest-order result to break down before this condition is reached. The reason is that for times $\tau \sim \tau_K \sim \Lambda^{-1} e^{\pi v_F/\lambda_K}$ the higher-order corrections must begin to renormalize the effective Kondo coupling. In fact, the finite time in the quench dynamics plays the role of an effective temperature $T_{\text{eff}} \sim 1/\tau$, which cuts off the infrared singularities associated with the Kondo effect, see Ref. [15]. To estimate the Kondo time scale, we set $\Lambda = 1$, $v_F = \sqrt{2}$ for $k_F = \pi/4$, and $\lambda_K = 1/2$, which gives $\tau_K \approx 7 \times 10^3$. Thus, in the same way that the Kondo screening cloud can reach mesoscopic length scales $\xi_K \sim 1 \mu\text{m}$ [11], the Kondo time is much longer than the microscopic

time scale set by the exchange coupling. In this work we focus on the regime $\Lambda^{-1} \lesssim \tau \ll \tau_K$, in which perturbation theory is under control and the dynamics is governed by the ultraviolet (weak coupling) fixed point of the Kondo problem. This is the relevant regime for comparison with the numerical results in Sec. IV and possibly with future experiments that might probe the nonequilibrium dynamics in this kind of quench protocol [27]. At long times, $\tau \gg \tau_K$, the dynamics must be governed by the low-energy fixed point at which the impurity spin is completely screened by the conduction electrons [37,39].

For the case where the impurity is coupled to both wires, we apply second-order perturbation theory in the Kondo coupling in Eq. (25). We obtain Eq. (30) with the correlator $C(\tau)$ replaced by $\langle F(\tau)F^\dagger(0) \rangle_0$. Once again, the spin relaxation is related to the correlator for the operators associated with spin-flip scattering in the Kondo interaction. In fact, the operator G in Eq. (27) does not appear in this lowest-order result. Leaving the details of the calculation to Appendix, here we write down the result:

$$m_0(\tau) = \frac{1}{2} - 2 \left(\frac{\lambda_K}{4\pi\alpha\Lambda} \right)^2 \left(\ln[1 + (\Lambda\tau)^2] + \frac{2\mathcal{C}^2 K_c^2}{1 - K_c} \left\{ 1 - [1 + (\Lambda\tau)^2]^{\frac{K_c-1}{2K_c}} \cos \left[\frac{1 - K_c}{K_c} \arctan(\Lambda\tau) \right] \right\} \right) + \mathcal{O}(\lambda_K^3). \quad (32)$$

The logarithmic term in this case differs by a factor of 2 from the corresponding term in Eq. (31). The decay is also enhanced by the contribution from the tunneling terms, which depends on Luttinger parameter K_c . Note that the exponent $1 - K_c^{-1}$ is negative for $K_c < 1$, which means that the power law vanishes for $\tau \rightarrow \infty$ and the term $\propto \mathcal{C}^2$ converges to a finite value. This happens because the tunneling operators in Eq. (26) have scaling dimension $(1 + K_c^{-1})/2$ and are irrelevant at tree level for repulsive interactions [39,51]. Therefore, the relaxation of the impurity magnetization is still predominantly driven by the marginal terms in the Kondo interaction, which give rise to the logarithmic term in Eq. (32). In the noninteracting limit $K_c \rightarrow 1$, the tunneling operators become marginal as well, and Eq. (32) reduces to the pure logarithmic dependence (setting $\mathcal{C} = 1$):

$$m_0(\tau) = \frac{1}{2} - 4 \left(\frac{\lambda_K}{4\pi\alpha\Lambda} \right)^2 \ln[1 + (\Lambda\tau)^2]. \quad (33)$$

This is expected because in this case the Kondo interaction in Eq. (23) can be rewritten in terms of the coupling to a single noninteracting channel, $H_K^{(2)} = 2\lambda_K \mathbf{S}_0 \cdot \psi_+^\dagger(0)(\sigma/2)\psi_+(0)$, where $\psi_+ = (\psi_1 + \psi_2)/\sqrt{2}$ annihilates an electron in the symmetric orbital.

IV. NUMERICAL RESULTS

In this section, we use tDMRG to study the nonequilibrium dynamics following a hybridization quench described by the Hamiltonian in Eq. (1). The numerical results were obtained using a second-order Suzuki-Trotter decomposition with a time step $d\tau = 0.05$, which keeps the error of the order of 10^{-6} for the time intervals we consider. In the preparation of the initial state, we fix the electron density at quarter filling, $\rho = 0.5$, by adjusting the chemical potential in the chains.

To simulate the dynamics for $\tau > 0$, we set the hybridization parameters $t'_{1,2} = 0.5$. In our DMRG method it is convenient to choose an even number of sites for the coupled system. For both geometries, we have fixed the total length to $L = 48$ sites. When the impurity is coupled to a single chain, we use $L_1 = 0$ and $L_2 = 47$. When both chains are included, we take $L_1 = 23$ and $L_2 = 24$. To lift the Kramers degeneracy in the initial state of the odd-length chain, we apply a weak magnetic field at the site farthest from the impurity spin. The small difference between the chains in the second geometry accounts for a slight asymmetry in the propagation of charge, spin, and entanglement in Fig. 2 below.

A. Light cones

After the local quench, the propagation of perturbations away from the impurity site is bounded by light cones [52]. It is known that low-lying excitations on top of the ground state can rule the velocities of the light cones [53]. For noninteracting leads, $U = 0$, the elementary excitations are electrons that carry both spin and charge simultaneously. By contrast, for $U > 0$, the exact solution of the one-dimensional Hubbard

TABLE I. Velocities and Luttinger parameter obtained from the Bethe ansatz solution of the Hubbard model at quarter filling for different values of the interaction U . Here v_{max} refers to the maximum velocity calculated from the exact holon dispersion.

U	v_s	v_c	v_{max}	K_c
2	1.09	1.67	2.06	0.82
4	0.86	1.81	2.05	0.71
8	0.56	1.93	2.02	0.62

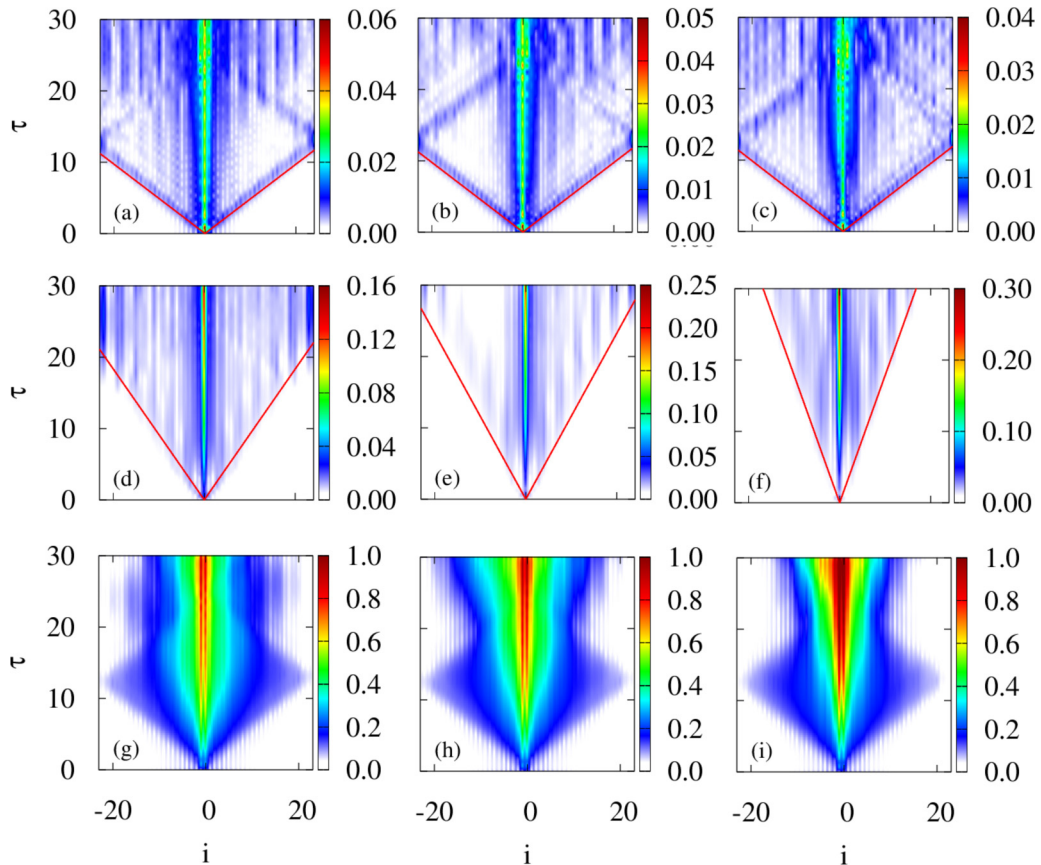


FIG. 2. Spatiotemporal dependence of local observables and entanglement entropy after the hybridization quench. Here we fix $U_d = 7$. Different columns correspond to different values of the interaction in the Hubbard chains: $U = 2$ (left panels), $U = 4$ (middle panels), and $U = 8$ (right panels). Panels in the same row show the variation in the local density $\Delta\rho(i, \tau)$ [(a)–(c)], local magnetization $m(i, \tau)$ [(d)–(f)], and entanglement entropy $\Delta S(i, \tau)$ [(g)–(i)]. Solid red lines represent the boundaries of the light cones defined by the maximum holon velocity v_{\max} for $\Delta\rho(i, \tau)$ in the top row and by the spin velocity v_s for $\Delta m(i, \tau)$ in the middle row, as given in Table I.

model tells us that the elementary excitations are spinons, which carry spin, holons, and antiholons, which carry charge and bound states thereof [47]. We may then anticipate that the light cone velocities in our quench protocol can be extracted from the dispersion of spinons and holons in the chains. Importantly, these are bulk properties which do not depend on the parameters at the impurity site.

We calculate the exact holon and spinon dispersions at quarter filling by solving the Bethe ansatz integral equations in the thermodynamic limit following Ref. [47]. Within the Bethe ansatz solution, the ground state is constructed by filling up the spinon and holon states with quantum numbers up to some values, fixed by electron density and magnetization, which define the Fermi boundary. At zero magnetic field, the maximum spinon velocity occurs at the Fermi boundary and can be identified with the spin velocity v_s in the TLL theory. On the other hand, the charge velocity v_c , calculated from low-energy particle-hole excitations in the holon dispersion, is not the maximum velocity for holons. The reason is that for any density below half filling the inflection point of the holon dispersion lies above the Fermi boundary. Here it is instructive to recall that this is also true for $U = 0$, where the free electrons have dispersion $\varepsilon_0(k) = -2 \cos k$. The maximum velocity in the band is $v_{\max} = \max\{d\varepsilon_0/dk\} = 2$, defined from single-particle states at $k = \pi/2$, which is higher than the Fermi

velocity $v_F = 2 \sin k_F = \sqrt{2}$ for $k_F = \pi/4$. Remarkably, in the opposite limit $U \rightarrow \infty$, the maximum velocity is also $v_{\max} = 2$, but here it comes from the dispersion of holons which behave as free spinless fermions [48]. In Table I, we show the values of the spin (v_s), charge (v_c), and maximum (v_{\max}) velocities calculated by Bethe ansatz for three different values of U . Note that $v_{\max} \approx 2$ for all values of the interaction. We stress that TLL theory does not predict v_{\max} , as the latter depends on the holon dispersion at finite energies.

In Fig. 2, we show the tDMRG results for perturbations in three different quantities as a function of position i and time τ after the quench when the impurity is coupled to both wires. Let us first discuss the change in the local density,

$$\Delta\rho(i, \tau) = |\langle\Psi(\tau)|n_i|\Psi(\tau)\rangle - \langle\Psi_0|n_i|\Psi_0\rangle|, \quad (34)$$

shown in panels (a)–(c) for $U = 2, 4, 8$, respectively, and fixed $U_d = 7$. Since this observable depends on charge fluctuations, its dynamics should be dominated by the propagation of holons. The slope of the red lines represented in Figs. 2(a)–2(c) is set by v_{\max} given in Table I, in good agreement with the observed light cones. Note that the fastest holons reach the open boundaries of the finite chains at time $\tau \approx 12$. After this, a second cone associated with reflection at the boundaries propagates back towards the center of the system. If we are

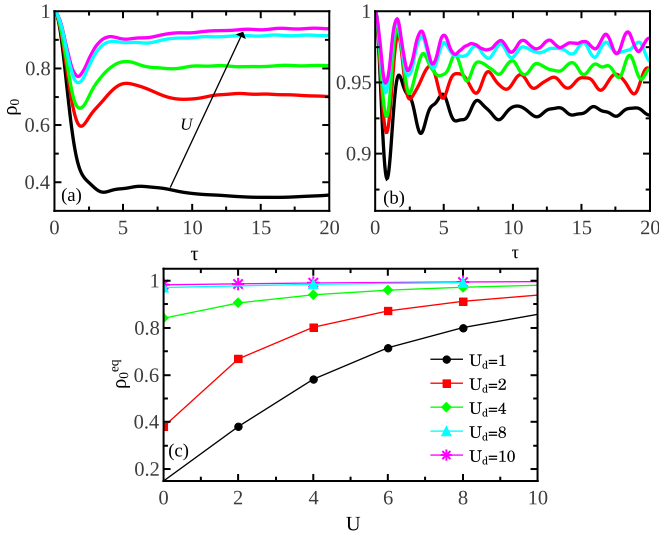


FIG. 3. Local occupation at the impurity site coupled to two wires. After the hybridization quench, the occupation varies in time as shown in (a) for $U_d = 2$ and in (b) for $U_d = 7$. Different curves in (a) and (b) correspond to different values of the interaction strength U in the chains; from bottom to top, $U = 0, 2, 4, 8, 10$. Panel (c) shows the equilibrium occupation as a function of U for different U_d for comparison with the dynamics.

interested in the behavior of local observables in the thermodynamic limit, we must restrict the measurement to times below this reflection cone.

Next, we consider the variation in the local magnetization,

$$\Delta m(i, \tau) = |\langle \Psi(\tau) | S_i^z | \Psi(\tau) \rangle - \langle \Psi_0 | S_i^z | \Psi_0 \rangle|. \quad (35)$$

In particular, $\Delta m(0, \tau) = 1/2 - m_0(\tau)$ corresponds to the decay of the impurity magnetization. The numerical result is shown in Figs. 2(d)–2(f). In this case, the slope of the light cone boundary is defined by the spin velocity v_s , which decreases with increasing interaction. Recall that $v_s \sim 1/U \rightarrow 0$ for $U \rightarrow \infty$. Clearly, in the strongly interacting limit perturbations in the spin sector propagate more slowly than perturbations in the charge sector, cf. panels (a)–(c).

Finally, we study how the von Neumann entanglement entropy (EE) evolves after the quench. Here we divide the system into two partitions, A and B, such that subsystem A comprises the leftmost i sites, while B contains the $L - i$ rightmost sites. The EE is defined as $S(i, \tau) = -\sum_n \xi_n \log \xi_n$, where $\{\xi_n\}$ is the set of eigenvalues of the reduced density matrix $\hat{\rho}_{A/B}(\tau) = \text{Tr}_{B/A} |\Psi(\tau)\rangle \langle \Psi(\tau)|$. In Figs. 2(g)–2(i), we show the propagation of variations in the EE, given by $\Delta S(i, \tau) = |S(i, \tau) - S(i, 0)|$. We observe that the velocity of the light cone in the entanglement entropy is close to v_{\max} , indicating that entanglement propagates with the velocity of the fastest excitation.

B. Local observables at the impurity site

Let us now investigate the time evolution of local observables at the impurity site. Figures 3(a) and 3(b) display the occupation number $\rho_0(\tau) = \langle \Psi(\tau) | n_0 | \Psi(\tau) \rangle$ for two different values of U_d and several values of U when the impurity is coupled to both wires. For comparison, in Fig. 3(c) we plot

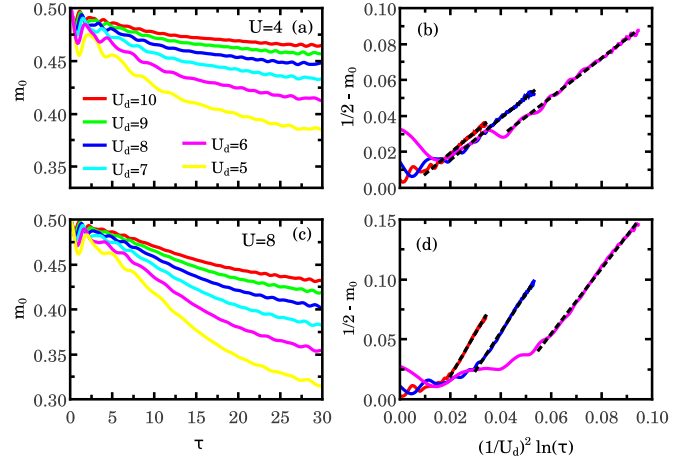


FIG. 4. Impurity magnetization as a function of time after the quench when the impurity spin is coupled to a single chain. (a) For fixed $U = 4$, the magnetization decays more slowly with increasing U_d . (b) For times $\tau \gtrsim 10$, the variation in the magnetization scales logarithmically with time. Panels (c) and (d) show the same as (a) and (b) for $U = 8$. The different slopes of the dashed lines in (b) and (d) show that the prefactor of the logarithmic time dependence increases with U .

the corresponding equilibrium values ρ_0^{eq} calculated from the ground state of the post-quench Hamiltonian in Eq. (1). Our results indicate that $\rho_0(\tau)$ approaches the equilibrium values for all values of U and U_d , but it also exhibits oscillations with a frequency that increases with U_d . Most importantly, we observe that the deviation from single occupancy $\Delta \rho_0 = 1 - \rho_0$ decreases as we increase both U_d and U , in agreement with the equilibrium results of Ref. [44]. This implies that the repulsive interaction in the chains facilitates the Kondo regime, where we can neglect charge fluctuations at the impurity site.

Now we focus on results for $U_d \geq 5$ to ensure that the system is close to the Kondo regime and analyze the decay of the impurity magnetization $m_0(\tau)$. We first discuss the geometry where the impurity is coupled to a single chain, for which we have the simpler analytical expression in Eq. (31). Figure 4 shows $m_0(\tau)$ for two values of U and several values of U_d . The numerical result shows oscillations at short times and also for $\tau \gtrsim 25$. The latter can be attributed to the finite size effect of reflection at the boundaries. Remarkably, the impurity magnetization decays faster with increasing U even though the spin velocity v_s decreases with U . Note that the total magnetization of the system is conserved due to the SU(2) symmetry of the Hamiltonian, which implies that $m_0(\tau)$ can only decay because the magnetization gets transported away from the impurity. However, the dynamics of the impurity magnetization has a qualitatively different interaction dependence than the ballistic propagation along the light cone.

At intermediate times, we observe a smooth behavior which can be compared with the field theory prediction. Approximating Eq. (31) for $\tau \gg \Lambda^{-1}$ and substituting $\lambda_K = 16(t'_2)^2/U_d$, we can write

$$\Delta m(0, \tau) \approx \frac{A}{U_d^2} \ln \tau + \text{const.}, \quad (36)$$

TABLE II. Fitting parameters for the decay of the impurity magnetization. The nonuniversal prefactor A is obtained by fitting the tDMRG results for a single chain to Eq. (36). Having fixed A , we determine B and C in Eq. (37) by fitting the data for two chains. The errors were estimated by varying the time intervals in the fitting.

U_d	$U = 4$		
	A	B	C
10	1.18 ± 0.03	0.36 ± 0.07	0.15 ± 0.03
8	1.17 ± 0.04	0.48 ± 0.02	0.20 ± 0.01
6	1.10 ± 0.06	0.62 ± 0.04	0.26 ± 0.02
U_d	$U = 8$		
	A	B	C
10	3.57 ± 0.08	0.71 ± 0.04	0.09 ± 0.01
8	3.3 ± 0.1	0.80 ± 0.08	0.09 ± 0.01
6	2.7 ± 0.9	0.79 ± 0.01	0.04 ± 0.01

where $A = 32(t'_2)^4/(\pi\alpha\Lambda)^2$ is a nonuniversal prefactor. In Figs. 4(b) and 4(d) we plot $\Delta m(0, \tau)$ versus $U_d^{-2} \ln \tau$. The results are in agreement with the logarithmic scaling expected for $\Lambda^{-1} \ll \tau \ll \tau_K$. Note that the parameter A (see Table II) controls the slope of the lines in the semilog plot. The fact that A remains approximately constant for the larger values of U_d confirms the dependence of the Kondo coupling $\lambda_K \sim 1/U_d$ for $t'_2 \ll U_d$. On the other hand, A clearly increases with the interaction U in the chains. This dependence is not predicted by TLL theory and must be associated with a renormalization of the cutoff parameters by bulk interactions. We also note that the logarithmic scaling at intermediate times demonstrated by our results differs from the exponential decay postulated in Ref. [30].

The decay of the impurity magnetization for the two-wire geometry is shown in Fig. 5. In the regime $\tau \gg \Lambda^{-1}$, the expression in Eq. (32) simplifies to

$$\Delta m(0, \tau) \approx \frac{2A}{U_d^2} \ln \tau - B\tau^{1-K_c^{-1}} + C, \quad (37)$$

where the Luttinger parameter K_c is known from Bethe ansatz (see Table I) and A , B , and C are nonuniversal parameters. Unfortunately, within the limited time range available numerically we are not able to unambiguously distinguish between a pure logarithmic dependence, as expected for the noninteracting case in Eq. (33), and the combination of a logarithm

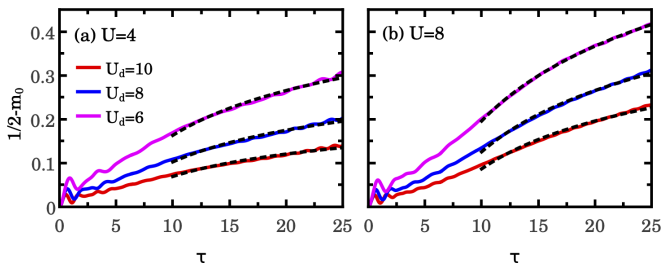


FIG. 5. Impurity magnetization when the impurity spin is coupled to both chains. The results are for (a) $U = 4$, (b) $U = 8$. The dashed lines represent the fittings to Eq. (37) with the parameters given in Table II.

and a power law with exponent $1 - K_c^{-1}$. We have fitted the data in Fig. 5 using Eq. (37) fixing K_c from Bethe ansatz and assuming that A takes the same value as in the single-wire geometry, see Fig. 4. The parameter B and C were left as fitting parameters. The result of this fitting is represented by the dashed lines in Fig. 5. The nonuniversal prefactors are of order 1 and are given in Table II. Overall, the numerical results are consistent with the analytical expressions.

V. CONCLUSIONS

We investigated the role of electronic interactions on the dynamic screening of a localized spin coupled to one-dimensional metallic leads. We considered a quantum quench in which a magnetic impurity is suddenly connected to interacting chains described by the Hubbard model. We studied the model numerically via the time-dependent density matrix renormalization group (tDMRG) formalism, as well as analytically within Tomonaga-Luttinger liquid (TLL) theory. Such a theoretical framework gives us access to the evolution of the system at intermediate timescales in regard to the formation of the Kondo screening cloud.

We have observed clear signatures of spin-charge separation in the propagation of density and magnetization pulses after the quench. The propagation is bounded by light cones with velocities that can be extracted from the dispersion relation of the elementary excitations. For densities below half filling, the fastest excitation is a holon with a finite energy above the Fermi level, whose velocity is higher than the charge velocity used in TLL theory. This maximum velocity defines the density light cone, while the maximum spinon velocity bounds the magnetization propagation. According to our tDMRG results, the propagation of the entanglement entropy, a nonlocal quantity, is also bounded by the maximum holon velocity.

Concerning local quantities at the impurity site, our results are consistent with relaxation towards the equilibrium values after the local quench. In particular, the relaxation of the impurity magnetization happens more rapidly if we decrease the interaction U_d at the impurity site, thereby enhancing the Kondo coupling, or if we increase the interaction in the chains. While the TLL theory predicts some interaction dependence through the charge Luttinger parameter when the impurity is coupled to two leads, we find that the most important interaction dependence comes from a renormalization of the nonuniversal prefactors. In the case of coupling to a single chain, the field theory predicts a logarithmic scaling in the perturbative regime of times shorter than the inverse Kondo temperature, which agrees well with our tDMRG results.

One interesting question that we leave to future work is what happens in the longtime limit, where the spin relaxation must be governed by the low-energy fixed point of the Kondo problem. This regime is hard to access by numerical techniques such as tDMRG, but one might search for a crossover in the time dependence analogous to the spatial dependence of spin correlations in the Kondo screening cloud [9,10]. It would also be instructive to consider other geometries, for instance by coupling the impurity site to the middle of a single chain, as in the original studies of the Kondo effect in Tomonaga-Luttinger liquids [36,37].

ACKNOWLEDGMENTS

We thank Marco Schiró for pointing out his work [42] and for suggesting that a similar calculation could be done for a spinful model. We acknowledge financial support from Conselho Nacional de Desenvolvimento Científico e Tecnológico, in particular CNPq INCT-IQ, CAPES, and FAPEMIG. Research at IIP-UFRN is supported by Brazilian ministries MEC and MCTI.

APPENDIX: CALCULATION OF THE TIME-DEPENDENT IMPURITY MAGNETIZATION

In this Appendix we provide details of the calculation of $m_0(\tau)$ in the field theory approach. Expanding the exponential function in Eq. (29) up to second order in λ_K , the expectation value of S_0^z becomes

$$\begin{aligned} m_0(\tau) &= \frac{1}{2} + i \int_0^\tau d\tau' \langle [H_K(\tau'), S_0^z(\tau)] \rangle_0 \\ &\quad - \frac{1}{2} \int_0^\tau d\tau' d\tau'' \{ \langle S_0^z(\tau) T[H_K(\tau')H_K(\tau'')] \rangle_0 \\ &\quad + \langle \tilde{T}[H_K(\tau')H_K(\tau'')] S_0^z(\tau) \rangle_0 \\ &\quad - 2 \langle H_K(\tau') S_0^z(\tau) H_K(\tau'') \rangle_0 \}, \end{aligned} \quad (\text{A1})$$

where T (\tilde{T}) is the time (antitime) ordering operator and we omit the lower index I for operators evolved in the interaction picture. Considering H_K given by Eq. (25), it is straightforward to show that

$$\langle [H_K(\tau'), S_0^z(\tau)] \rangle_0 = 0, \quad (\text{A2})$$

since $[S_0, H_0] = 0$ for $H_0 = \sum_\ell H_\ell^{\text{LL}}$. Thus, the first-order term vanishes identically.

In the second-order terms, it is important to keep track of the time ordering in the product of impurity spin operators since

$$\langle T S_0^+(\tau') S_0^-(\tau'') \rangle_0 = \Theta(\tau' - \tau''), \quad (\text{A3})$$

$$\langle T S_0^-(\tau') S_0^+(\tau'') \rangle_0 = \Theta(\tau'' - \tau'). \quad (\text{A4})$$

Similar expressions hold for \tilde{T} . For the two-wire geometry, the $\mathcal{O}(\lambda_K^2)$ terms in the expansion are given by

$$\begin{aligned} \langle S_0^z(\tau) T[H_K(\tau')H_K(\tau'')] \rangle_0 &= \left(\frac{\lambda_K}{2} \right)^2 \left\{ \frac{1}{8} \langle T G(\tau') G(\tau'') \rangle_0 \right. \\ &\quad + \frac{\theta(\tau' - \tau'')}{2} \langle F(\tau') F^\dagger(\tau'') \rangle_0 \\ &\quad \left. + \frac{\theta(\tau'' - \tau')}{2} \langle F(\tau'') F^\dagger(\tau') \rangle_0 \right\}, \end{aligned} \quad (\text{A5})$$

$$\begin{aligned} \langle \tilde{T}[H_K(\tau')H_K(\tau'')] S_0^z(\tau) \rangle_0 &= \left(\frac{\lambda_K}{2} \right)^2 \left\{ \frac{1}{8} \langle \tilde{T} G(\tau') G(\tau'') \rangle_0 \right. \\ &\quad + \frac{\theta(\tau' - \tau'')}{2} \langle F(\tau'') F^\dagger(\tau') \rangle_0 \\ &\quad \left. + \frac{\theta(\tau'' - \tau')}{2} \langle F(\tau') F^\dagger(\tau'') \rangle_0 \right\}, \end{aligned} \quad (\text{A6})$$

$$\begin{aligned} \langle H_K(\tau') S_0^z(\tau) H_K(\tau'') \rangle_0 &= \left(\frac{\lambda_K}{2} \right)^2 \left\{ \frac{1}{8} \langle G(\tau') G(\tau'') \rangle_0 - \frac{1}{2} \langle F(\tau') F^\dagger(\tau'') \rangle_0 \right\}. \end{aligned} \quad (\text{A7})$$

After some algebra, we obtain

$$\begin{aligned} m_0(\tau) &= \frac{1}{2} - \left(\frac{\lambda_K}{2} \right)^2 \int_0^\tau d\tau' d\tau'' \{ \langle F(\tau') F^\dagger(\tau'') \rangle_0 \\ &\quad + \frac{1}{16} \langle [G(\tau''), G(\tau')] \rangle_0 \}. \end{aligned} \quad (\text{A8})$$

The last term in the integral vanishes since the commutator is antisymmetric under the exchange $\tau' \leftrightarrow \tau''$. Therefore, the second-order contribution only involves the correlator for the operator $F(\tau)$.

The correlator can be written in the form

$$\langle F(\tau') F^\dagger(\tau'') \rangle_0 = \left(\frac{2}{\pi\alpha} \right)^2 C_1(\tau' - \tau'') C_2(\tau' - \tau''). \quad (\text{A9})$$

The first factor only involves the spin bosons:

$$\begin{aligned} C_1(\tau) &= \langle e^{-i\sqrt{\frac{\pi}{2}}\phi_{1s}(\tau)} e^{i\sqrt{\frac{\pi}{2}}\phi_{1s}(0)} \rangle_0 \langle e^{-i\sqrt{\frac{\pi}{2}}\phi_{2s}(\tau)} e^{i\sqrt{\frac{\pi}{2}}\phi_{2s}(0)} \rangle_0 \\ &= \frac{1}{1 + i\Lambda\tau}, \end{aligned} \quad (\text{A10})$$

where we used $K_s = 1$ and introduced the high-energy cutoff Λ . The second factor involves both charge and spin bosons:

$$\begin{aligned} C_2(\tau) &= \frac{1}{8} \{ \langle e^{i\sqrt{\frac{\pi}{2}}\phi_{1c}(\tau)} e^{-i\sqrt{\frac{\pi}{2}}\phi_{1c}(0)} \rangle_0 \times [1 \rightarrow 2] \\ &\quad + \langle e^{i\sqrt{\frac{\pi}{2}}\phi_{1s}(\tau)} e^{-i\sqrt{\frac{\pi}{2}}\phi_{1s}(0)} \rangle_0 \times [1 \rightarrow 2] \} \\ &= \frac{1}{8} \left[\frac{1}{(1 + i\Lambda\tau)^{\frac{1}{k_c}}} + \frac{1}{1 + i\Lambda\tau} \right]. \end{aligned} \quad (\text{A11})$$

Finally, the correlator in Eq. (A9) can be written as

$$\begin{aligned} \langle F(\tau') F^\dagger(\tau'') \rangle_0 &= \frac{1}{2\pi^2\alpha^2} \left\{ \frac{1}{[1 + i\Lambda(\tau' - \tau'')]^{\frac{1}{k_c} + 1}} \right. \\ &\quad \left. + \frac{1}{[1 + i\Lambda(\tau' - \tau'')]^2} \right\}. \end{aligned} \quad (\text{A12})$$

[1] A. Hewson, *The Kondo Problem to Heavy Fermions*, Cambridge Studies in Magnetism (Cambridge University Press, Cambridge, 1997).

[2] K. G. Wilson, *Rev. Mod. Phys.* **47**, 773 (1975).

[3] N. Andrei, K. Furuya, and J. H. Lowenstein, *Rev. Mod. Phys.* **55**, 331 (1983).

- [4] I. Affleck and A. W. Ludwig, *Nucl. Phys. B* **360**, 641 (1991).
- [5] P. Nozières, *J. Low Temp. Phys.* **17**, 31 (1974).
- [6] J. E. Gubernatis, J. E. Hirsch, and D. J. Scalapino, *Phys. Rev. B* **35**, 8478 (1987).
- [7] T. Hand, J. Kroha, and H. Monien, *Phys. Rev. Lett.* **97**, 136604 (2006).
- [8] V. Barzykin and I. Affleck, *Phys. Rev. Lett.* **76**, 4959 (1996).
- [9] L. Borda, *Phys. Rev. B* **75**, 041307(R) (2007).
- [10] A. Holzner, I. P. McCulloch, U. Schollwöck, J. von Delft, and F. Heidrich-Meisner, *Phys. Rev. B* **80**, 205114 (2009).
- [11] I. Affleck, *Perspectives of Mesoscopic Physics - Dedicated to Yoseph Imry's 70th Birthday*, edited by A. Aharony and O. Entin-Wohlmann (World Scientific, Singapore, 2010), pp. 1–44.
- [12] I. V. Borzenets, J. Shim, J. C. H. Chen, A. Ludwig, A. D. Wieck, S. Tarucha, H. S. Sim, and M. Yamamoto, *Nature (London)* **579**, 210 (2020).
- [13] D. Goldhaber-Gordon, H. Shtrikman, D. Mahalu, D. Abusch-Magder, U. Meirav, and M. A. Kastner, *Nature (London)* **391**, 156 (1998).
- [14] S. M. Cronenwett, T. H. Oosterkamp, and L. P. Kouwenhoven, *Science* **281**, 540 (1998).
- [15] P. Nordlander, M. Pustilnik, Y. Meir, N. S. Wingreen, and D. C. Langreth, *Phys. Rev. Lett.* **83**, 808 (1999).
- [16] J. Paaske, A. Rosch, and P. Wölfle, *Phys. Rev. B* **69**, 155330 (2004).
- [17] F. B. Anders and A. Schiller, *Phys. Rev. Lett.* **95**, 196801 (2005).
- [18] S. Kehrein, *Phys. Rev. Lett.* **95**, 056602 (2005).
- [19] M. Pletyukhov and H. Schoeller, *Phys. Rev. Lett.* **108**, 260601 (2012).
- [20] H. E. Türeci, M. Hanl, M. Claassen, A. Weichselbaum, T. Hecht, B. Braunecker, A. Govorov, L. Glazman, A. Imamoglu, and J. von Delft, *Phys. Rev. Lett.* **106**, 107402 (2011).
- [21] H. T. M. Nghiem and T. A. Costi, *Phys. Rev. Lett.* **119**, 156601 (2017).
- [22] K. Wrzesniewski and I. Weymann, *Phys. Rev. B* **100**, 035404 (2019).
- [23] I. Krivenko, J. Kleinhenz, G. Cohen, and E. Gull, *Phys. Rev. B* **100**, 201104(R) (2019).
- [24] J. Bauer, C. Salomon, and E. Demler, *Phys. Rev. Lett.* **111**, 215304 (2013).
- [25] Y. Nishida, *Phys. Rev. Lett.* **111**, 135301 (2013).
- [26] L. Riegger, N. Darkwah Oppong, M. Höfer, D. R. Fernandes, I. Bloch, and S. Fölling, *Phys. Rev. Lett.* **120**, 143601 (2018).
- [27] M. Kanász-Nagy, Y. Ashida, T. Shi, C. P. Moca, T. N. Ikeda, S. Fölling, J. I. Cirac, G. Zaránd, and E. A. Demler, *Phys. Rev. B* **97**, 155156 (2018).
- [28] M. Medvedyeva, A. Hoffmann, and S. Kehrein, *Phys. Rev. B* **88**, 094306 (2013).
- [29] B. Lechtenberg and F. B. Anders, *Phys. Rev. B* **90**, 045117 (2014).
- [30] M. Nuss, M. Ganahl, E. Arrigoni, W. von der Linden, and H. G. Evertz, *Phys. Rev. B* **91**, 085127 (2015).
- [31] R. Vasseur, K. Trinh, S. Haas, and H. Saleur, *Phys. Rev. Lett.* **110**, 240601 (2013).
- [32] D. M. Kennes, V. Meden, and R. Vasseur, *Phys. Rev. B* **90**, 115101 (2014).
- [33] S. Ghosh, P. Ribeiro, and M. Haque, *J. Stat. Mech.* (2015) P08002.
- [34] V. V. Deshpande, M. Bockrath, L. I. Glazman, and A. Yacoby, *Nature (London)* **464**, 209 (2010).
- [35] T. Giamarchi, *Quantum Physics in One Dimension* (Clarendon Press, Oxford, 2003).
- [36] D.-H. Lee and J. Toner, *Phys. Rev. Lett.* **69**, 3378 (1992).
- [37] A. Furusaki and N. Nagaosa, *Phys. Rev. Lett.* **72**, 892 (1994).
- [38] P. Fröjdh and H. Johannesson, *Phys. Rev. Lett.* **75**, 300 (1995).
- [39] M. Fabrizio and A. O. Gogolin, *Phys. Rev. B* **51**, 17827 (1995).
- [40] K. A. Hallberg and C. A. Balseiro, *Phys. Rev. B* **52**, 374 (1995).
- [41] R. Egger and A. Komnik, *Phys. Rev. B* **57**, 10620 (1998).
- [42] M. Schiró and A. Mitra, *Phys. Rev. B* **91**, 235126 (2015).
- [43] P. Simon and I. Affleck, *Phys. Rev. B* **68**, 115304 (2003).
- [44] S. Costamagna, C. J. Gazza, M. E. Torio, and J. A. Riera, *Phys. Rev. B* **74**, 195103 (2006).
- [45] A. Gogolin, A. Nersesyan, and A. Tsvelik, *Bosonization and Strongly Correlated Systems* (Cambridge University Press, Cambridge, 2004).
- [46] E. H. Lieb and F. Y. Wu, *Phys. Rev. Lett.* **20**, 1445 (1968).
- [47] F. Essler, H. Frahm, F. Göhmann, A. Klümper, and V. Korepin, *The One-Dimensional Hubbard Model* (Cambridge University Press, Cambridge, 2005).
- [48] M. Ogata and H. Shiba, *Phys. Rev. B* **41**, 2326 (1990).
- [49] H. Schulz, *Int. J. Mod. Phys. B* **05**, 57 (1991).
- [50] R. G. Pereira, N. Laflorencie, I. Affleck, and B. I. Halperin, *Phys. Rev. B* **77**, 125327 (2008).
- [51] S. Andergassen, T. Enss, and V. Meden, *Phys. Rev. B* **73**, 153308 (2006).
- [52] E. H. Lieb and D. W. Robinson, *Commun. Math. Phys.* **28**, 251 (1972).
- [53] A. L. de Paula, H. Bragança, R. G. Pereira, R. C. Drumond, and M. C. O. Aguiar, *Phys. Rev. B* **95**, 045125 (2017).